Formation of Planar Arrays of One-Dimensional p−n Heterojunctions Using Surface-Directed Growth of Nanowires and Nanowalls

Babak Nikoobakht* and Andrew Herzing

Surface and Microanalysis Science Division, National Institute of Standards and Technology, 100 Bureau Drive, Stop 8372, Gaithersburg, Maryland 20899

ABSTRACT We report a surface-directed vapor−liquid−solid process for planar growth of one-dimensional heterojunctions of zinc oxide on single crystal gallium nitride (GaN) that enables their hierarchical assembly to light emitting diodes. An individual heterojunction is about 10 μm in length and 80 nm in width and is formed by planar growth of an n-type ZnO nanowire or nanowall on p-type GaN surface using Au catalyst. Our results show that a ZnO nanocrystal at its nucleation site has six possible growth directions that can be engineered and controlled using an intentional blockade of the nanocrystal growth in certain directions owing to similarities in crystal structures of ZnO and GaN. The ZnO nanowalls are formed when nanowires during their planar growth slowly grow in direction normal to the substrate *via* a self-catalytic process. The crystal structure of these heterojunctions is examined from two different crystallographic perspectives using high resolution transmission electron microscopy. Results indicate abrupt and epitaxial formation of n−p heterojunctions, which are difficult to achieve in thin film growth of these heterojunctions. The collective light emission of micrometer- to millimeter-size arrays of the heterojunctions is demonstrated *via* a simple design that is scalable to literally any platform size. This technique allows *in situ* growth and combinations of II−VI and III−V semiconductors and offers their easier integration to photonic and lab-on-chip platforms with applications in energy generation and light detection.

KEYWORDS: surface-directed growth · directed assembly · nanowires · nanowalls · zinc oxide · p−n heterojunction

Despite significant advances in controlling the hierarchical order of semiconductor nanowires in recent years, the integration of highly ordered nanowire p−n junctions or field-effect transistors into electro-optical devices has proven to be increasingly complex due to the difficulty in controlling the position and orientation of microscopic arrays of nanowires on a large scale.[1−3] Thus far, the majority of semiconductor nanowires and their heterostructures have been grown *via* the VLS process in which a metal catalyst confines the nanocrystal growth resulting in the formation of free-standing nanowires. The strength of the VLS process is in the control of the composition, electronic structure, and morphology of the nanowires, and this has allowed the formation of, for instance, homo-, and heterojunctions with axial or core−shell junctions.[4−12] In free-standing electro-optical devices, typically heterojunctions are at the nanowire interface with the substrate[13,14] and in more complicated designs heterojunctions or quantum dots are fabricated along the nanowires.[15] Regardless of the position of the heterojunction in all these designs, a top contact is necessary to complete a typical device.

The fundamental limitation in integrating free-standing nanowires to *planar* devices is the need for the transfer and alignment of a massive number of nanowires to a receiver substrate with an inherent uncertainty in the position of each nanowire. This drawback has substantially hindered the development of electrically driven planar nanowire devices and light sources. So far the electrical injection has been limited to a small number of p−n junction nanowire devices.[16−18] To this end, a variety of properties such as capillary forces,[19] shear stress,[20] adhesion forces,[21,22] *etc.*, have been cleverly used to control the orientation of nanowires on a given surface; however, realization of architectures and circuitries comparable to the complexity of "top-down" nanoelectronics requires a precision and control beyond what has been offered so far.

Our efforts have been focused on addressing the main disadvantage of the VLS growth process by extending its use to planar growth of nanocrystals. To that effect, we previously showed the lateral ZnO growth on a-plane sapphire;[23] later the concept was shown for growth of GaAs nanowires on GaAs substrate.[24] In the present work, we extend this process to formation of high quality heterojunctions of II−VI and

*Address correspondence to babakn@nist.gov.

Received for review August 11, 2010 and accepted September 08, 2010.

Published online September 15, 2010.
10.1021/nn1019972

III−V semiconductors, a characteristic that has been challenging to realize in homo- and heterojunction growth of these semiconductors.[25,26]

In the traditional VLS process the nanocrystal growth is confined within a Au nanodroplet that dewets the substrate at early stages of the growth resulting in standing nanowires. In SVLS method, the nanodroplet stays in contact with the substrate during the growth allowing the substrate to guide the horizontal growth of the nanocrystal. As the nanocrystal grows, the Au nanodroplet also moves on the surface by maintaining its interface with the substrate and nanocrystal. This method preserves the advantages of the VLS process, while simultaneously allowing for careful control of the nanocrystal growth site and direction. To demonstrate this concept, we form addressable microarrays of p−n heterojunctions by lateral growth of n-type ZnO nanowires, a II−VI semiconductor with hexagonal structure, on a p-type GaN substrate with a similar crystal structure. The dramatic effect of the substrate on the lateral growth of nanowires is clearly shown in this system, and ways to control the large scale orientation of nanowires is discussed. ZnO, a wide band gap semiconductor, is attracting renewed interest for UV light emission and lasing, piezoelectric devices,[27] "invisible" circuitry,[28] and photovoltaics.[29] Its band gap can be engineered by the addition of Mg or Cd dopants, which are inexpensive and abundant.[30] ZnO also exhibits one of the highest exiton binding energies (~60 meV), which makes it a good candidate for high efficiency UV−visible light emitters. To this end, we show a simple device design that allows charge injection to a large number of laterally grown heterojunctions. These results are accompanied by high resolution transmission electron microscopy (HRETM), scanning electron microscopy (SEM), as well as optical microscopy to further reveal the properties of the grown heterojunctions. The reported approach could enable formation of a wide range of electrically addressable II−VI and III−V heterojunctions and their easier integration to photonic and lab-on-chip platforms with applications in energy generation and light detection.

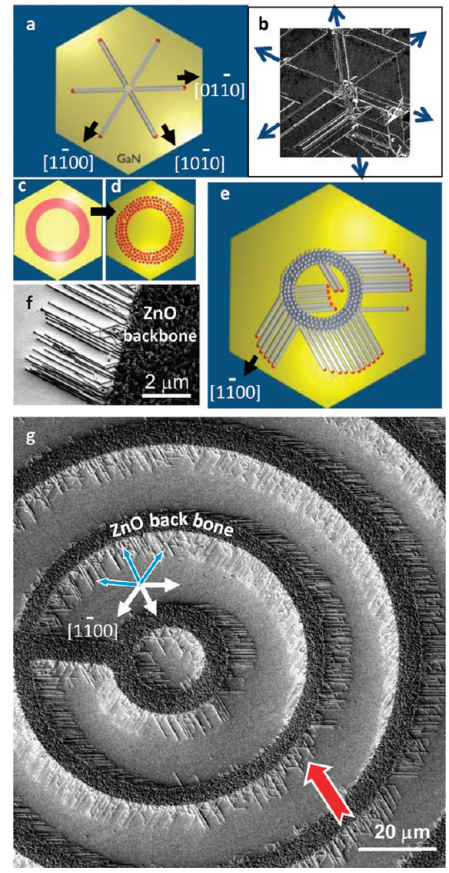

Figure 1. (a) Schematic showing the 6-fold symmetry of the surface-directed VLS growth of ZnO nanocrystals using Au nanoparticles (red circles) on *c*-plane GaN and (b) its corresponding micrograph illustrating these growth directions. (c) The circular drawing in red represents the Au pattern deposited on GaN *via* standard photolithography, which (d) converts to nanodroplets at elevated temperatures. (e) The Au nanodroplets at the boundaries of the circular pattern result in horizontal nanowires, but only grow in the three specific directions. (f) The SEM image of a group of ZnO nanowires horizontally grown at the border of a Au pattern; they are all connected to a ZnO thin film (called backbone). (g) The SEM image of arrays of p−n heterojunctions made from n-type ZnO nanowires grown on p-type GaN. Nanowires preferentially grow in three directions and are all electrically connected *via* the ZnO backbone that can be seen as the dark-gray circular pattern. The blue arrows highlight the growth directions that are suppressed due to the carrier gas flow direction (gas flow is shown with the red arrow).

RESULTS AND DISCUSSION

The lateral growth of ZnO takes place on a Au-patterned and c-plane GaN substrate. The process is carried out inside a tube furnace that is held at 900 °C, with the substrate being placed in a stream of ultradry N_2 carrier gas containing Zn and O precursors (Methods). The lateral growth of nanowires on GaN in the growth chamber found to be location sensitive as opposed to the growth of standing nanowires (Methods). At high temperature, the resulting Au nanodroplets promote the planar growth of ZnO nanocrystals *via* the SVLS process, which is influenced by the lattice match and crystal symmetry of the nanocrystals and the substrate. Crystal symmetry clearly demonstrates its effect in a system like ZnO (*a, b* = 0.32489 nm) on GaN (*a, b* = 0.31894 nm), which contains a lattice mismatch of ~1.8%. In the simplest case, we observed that by using 10−40 nm gold nanoparticles dispersed on GaN, the substrate directs the growth in six equivalent directions of $\langle 10\bar{1}0 \rangle$ with a hexagonal symmetry as shown in Figure 1a,b. The observed 6-fold symmetry confirms the contribution of the underlying substrate in determining the growth direction. The site selectivity of the growth is shown by Au patterning a GaN surface and growth of ZnO nanostructures. In this process, a photolithographically generated Au pattern with a thickness of 8 (±2) nm (Figure 1c) at elevated temperatures (500−700 °C) converts to packs of Au nanodroplets

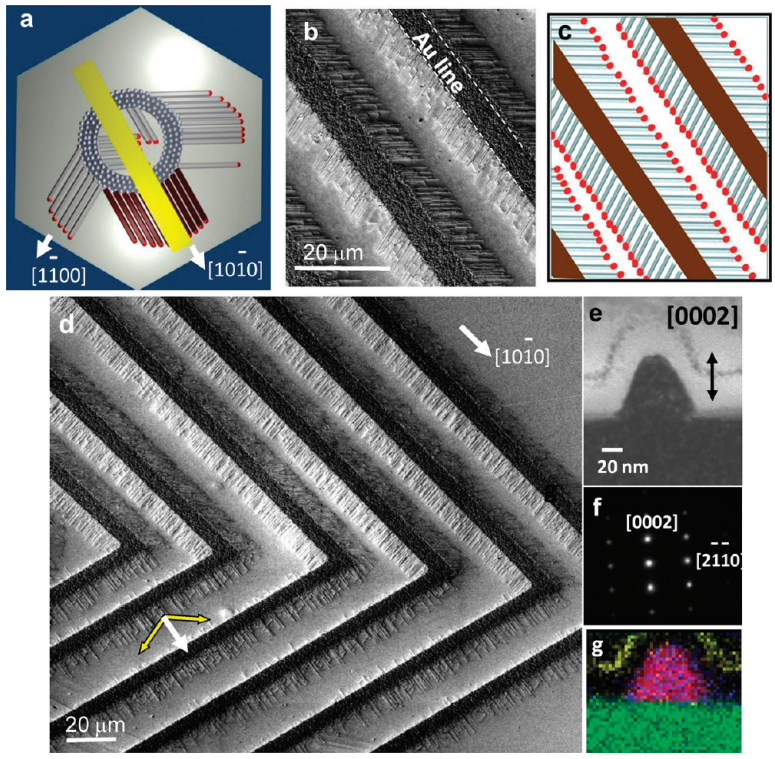

Figure 2. (a) Controlling the three growth directions of nanowires on GaN. Yellow line, schematically, represents a Au line deposited in the [10$\bar{1}$0] direction to just block the growth of nanowires in that direction (nanowires are shown in darker color). The two allowed growth directions are observed in the micrograph (b) and its corresponding schematic (c) further highlights this observation. (d) Micrograph showing the tilted view of an assembly of ZnO nanowires. The arrow at top part of the graph shows the [10$\bar{1}$0] direction of GaN. Au lines in this direction result in assembly of nanowires in two directions and Au lines perpendicular to this direction (bottom of the image) result in just one major nanowire growth direction (shown with white arrow). (e) TEM image of a faceted cross-section of a ZnO nanowire on GaN. (f) Elemental map of the cross-section in panel e constructed by XEDS elemental maps of Ga (green), Zn (red), O (blue), and Pt (yellow) XEDS signals. Pt residual originates from the Pt deposition during the specimen preparation. Image width is 100 nm and pixel size is 2 nm.

(Figure 1d). As shown in the drawing of Figure 1e and SEM image of Figure 1f, at a temperature range of 800−950 °C, while the ZnO phase transport is in progress, only Au nanodroplets formed at the perimeter of a Au pattern have the opportunity to laterally move on the substrate and form nanowires. The rest of the nanodroplets within the Au pattern result in standing nanowires and an underlying thin ZnO film[31−33] (hereafter, called ZnO backbone) by which all the horizontal nanowires are electrically connected to each other. Originally, the circular pattern in Figure 1e was anticipated to show all six growth directions of ZnO nanowires; however, as shown in the SEM image of Figure 1g, only three growth directions (white arrows) were observed. These three growth directions have one feature in common and that is being against the stream of the carrier gas containing Zn and O precursors (red arrow), meaning Au nanodroplets see the flow. When using large size Au patterns, we think the gas flow direction (red arrow) results in a shadowing effect caused by the faster growth of standing nanowires that mask a certain group of Au nanodroplets. These masking effects result in a very slow growth of nanowires in certain regions of the Au pattern leading to what we observe in Figure 1g.

The three dominant growth directions of nanowires in a given assembly can be controlled and engineered by application of Au catalyst lines along directions normal to *m*-planes of GaN. This concept is schematically illustrated in Figure 2a, with only the three growth directions of nanowires (under the current experimental condition) shown. In this design, Au nanodroplets at the perimeter of a Au pattern grow to nanowires *only if* the angle between the nanowire direction and the Au line at the point of nanowire growth is about 3° or more. Below this value, nanowires tend to merge with the ZnO backbone and are not observable. For this reason, in the example of Figure 2a, the Au line deposited in [10$\bar{1}$0] direction of GaN is expected to eliminate the growth direction of nanowires shown with the darker color. Experimentally, we observe two major growth directions for nanowires as seen in the SEM image of Figure 2b and its corresponding schematic (Figure 2c). Using the same principles, depositing Au lines *perpendicular* to the [10$\bar{1}$0] direction, as demonstrated in Figure 2d (bottom half of the image), causes suppression of two growth directions of [1$\bar{1}$00] and [01$\bar{1}$0]. This results in just one major nanowire growth direction as highlighted by the white arrow at the bottom of Figure 2d. Transmission electron microscopy (TEM)

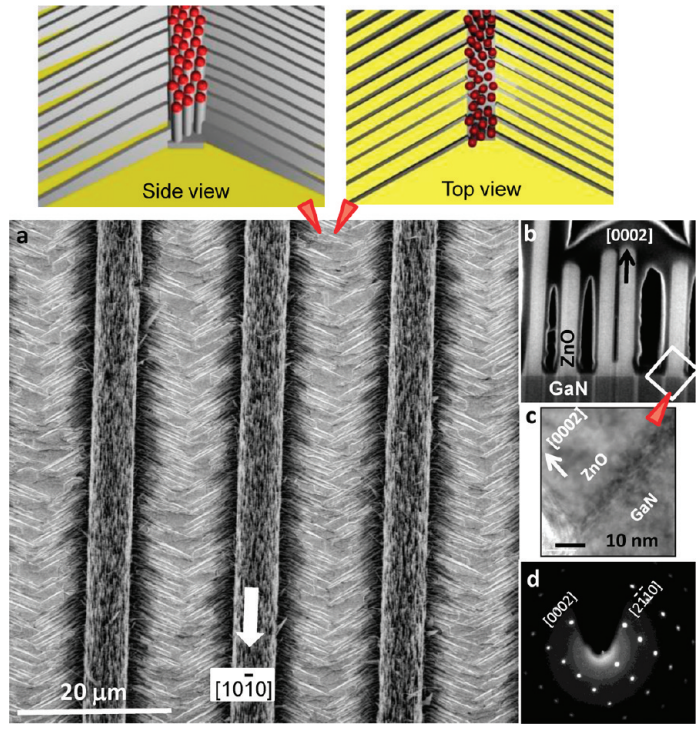

Figure 3. (a) Assemblies of ZnO nanowalls grown from periodic arrays of Au lines with a film thickness of 15(±2) nm and 5 mm length deposited along the [10$\bar{1}$0] GaN. The inset drawings show the side and top views of such arrays and the free-standing nanowires. (b) Micrograph of cross sections of a group of ZnO nanowalls shows that they grow in upright position with four major facets and a narrow width distribution of about 80 nm. (c) TEM image of a ZnO nanowall−GaN interface that is highlighted in part b and its corresponding selected area diffraction (SAD) pattern (d) shows that the out-of-plane growth direction of a ZnO nanowall is [0002]. Nanowalls from sides are enclosed to ±{2$\bar{1}\bar{1}$0} crystallographic facets.

examination of the cross-section of ZnO nanowires on GaN in Figure 2e shows a faceted ZnO nanocrystal with the selected area diffraction (SAD) pattern, shown in Figure 2f, indicting a single crystal structure with its [0002] and [2$\bar{1}\bar{1}$0] directions, respectively, normal and parallel to the basal plane (0001) of GaN. Elemental maps (Figure 2g and Supporting Information, Figure S1) acquired *via* X-ray energy dispersive spectroscopic (XEDS) imaging suggest that an abrupt junction exists between the ZnO and the GaN substrate.

The nanowire width stays constant during its lateral growth indicating that diffusion of Au to the nanowire facets and reduction in the volume of Au nanodroplets remain insignificant for nanodroplets smaller than 20 nm.[34] When the diameter of the Au nanodroplets increases above 20 nm, the nanowires acquire a new dimension by growing in $[0002]_{ZnO}$ direction normal to the substrate plane. Utilizing this observation, by depositing Au patterns with thickness of 10(±2) to 17(±2) nm, we are able to laterally grow ZnO nanowalls. Figure 3a is the side view of an assembly of ZnO nanowalls grown from a 5 mm × 5 mm array of parallel Au lines with 5 μm line width and 20 μm pitch. In this figure, Au line patterns are deposited parallel to [10$\bar{1}$0] of GaN in order to allow the lateral growth of ZnO nanowalls in only two directions of [01$\bar{1}$0] and [1$\bar{1}$00]; the inset schematics show the side and top views of nanowall arrays. Examining the cross sections of closely packed ZnO nanowalls (Figure 3b) shows they are vertical ZnO slabs with four dominant facets that can grow few micrometers in the direction normal to the interface. TEM and electron diffraction analyses of these ZnO cross sections, shown in Figure 3(c,d) indicate that nanowalls are single crystal and grow along their polar face in ± [0002] directions. Because of the large number of Au nanodroplets formed at the perimeter of each Au line, a high density of nanowalls can be grown that is an advantageous feature in applications such as photovoltaics and photodetection where the surface area is important. The height of a nanowall gradually decreases toward its leading end indicating that its vertical growth most likely is due to a slower self-catalytic process.[35] Previously, in the case of ZnO nanocantilevers, self-catalytic growth was attributed to the formation of Zn clusters on the (0002) polar surface of ZnO nanowires.[35] Since nanowalls are only observed in the case of larger-size Au nanodroplets, it seems that a vapor−solid growth including a self-catalytic one promotes the growth of the polar face of the ZnO in its [0002] direction.

The present technique is suitable for fabricating II−VI nanowire-based devices on III−V semiconductor substrates including GaN and its other combinations such as InGaN, AlGaN, *etc.* As an example, in Figure 4a, we demonstrate a simple strategy for fabricating arrays of electrically driven, light-emitting, p−n hetero-

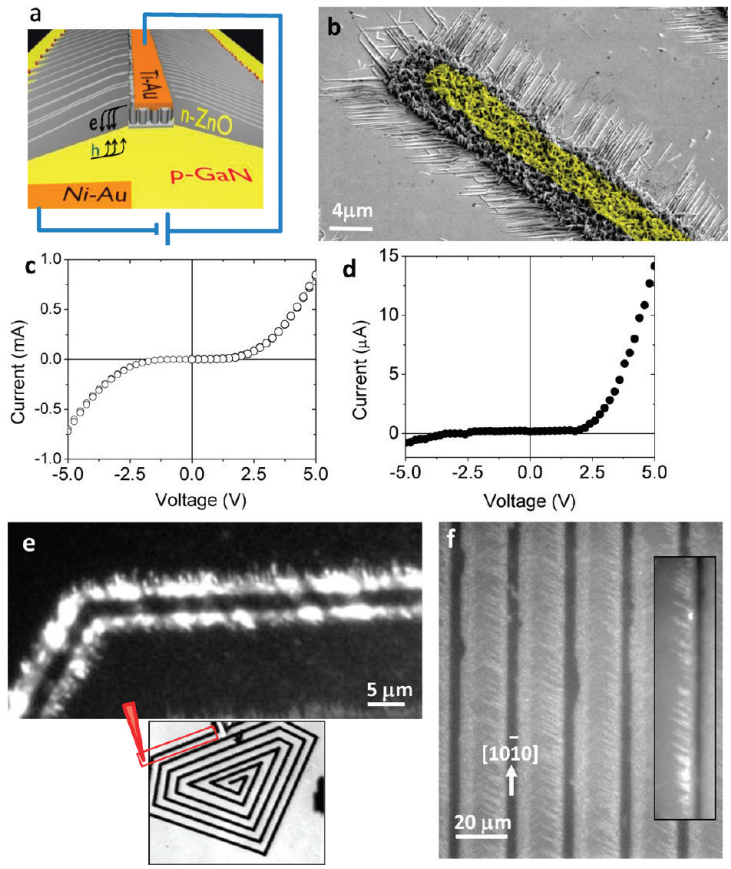

Figure 4. (a) Schematic showing the side view of an electrically driven array of p−n heterojunctions made from n-type ZnO nanowalls on p-type GaN. A micrograph of this device is illustrated in panel b, where the yellow color indicates the deposited metal electrode on the ZnO backbone. (c,d) I−V scans of two nanowall−LED devices, respectively, with 5 mm and 100 μm in dimension. (e) The electroluminescence image of a group of emitting p−n heterojunctions that is part of a millimeter-long nanowall array with a ZnO backbone in shape of a faceted spiral, which is shown in the optical image in the inset. In this example the injected current is ~0.9 mA at +7 V. (f) The electroluminescence image of a 5 mm-long array of emitting nanowall p−n heterojunctions with a 20 μm-pitch array spacing. The arrays are formed along the specified direction relative to the GaN *m*-planes. Inset shows the same array but emitting under a forward injection current of 0.02 A.

junctions formed at the interface between ZnO nanowires or nanowalls and the GaN substrate. Since the relative location of nanowire arrays are known, metal contacts can be readily deposited *via* standard photolithography over the ZnO backbones. A representative image of a three-layer (metal/ZnO nanowalls/GaN) structure is shown in Figure 4b, where the top metal electrode (Ti−Au) deposited on the ZnO backbone is highlighted in yellow (Supporting Information, Figure S2). During the device operation, the metal contacts on the ZnO backbones allow electron injection into nanowires or nanowalls and hole injection from the p-GaN side. The location, size, and shape of the light emitting devices can be controlled by depositing Au patterns ranging from a few micrometers to several millimeters with triangular, circular, and square shapes (Supporting Information, Figures S3 and S4).

Current−voltage (*I*−*V*) characteristics of the as grown p−n heterojunctions exhibit a rectifying behavior for small and large groups of nanowires or nanowalls. Multiple devices were repeatedly operated from −25 to 27 V in order to examine the structural and functional stability of the p−n heterojunctions. Results in Figure 4panels c,d, respectively, show the *I*−*V* scans of a 5 mm × 5 mm n−p heterojunction array and a 100 μm-size array. The amount of injected current is substantially larger in larger size devices, due to the larger number of involved nanowires as well as the contribution of the ZnO backbone in conducting the charges to the GaN layer. We typically observe turn-on voltages of 2.7−3.8 (±0.2), breakdown voltages of 3−9 V, and diode ideality factors ranging from 3−3.4 (Supporting Information, Figure S4), which are comparable to those of free-standing heterojunction nanowires.[16] In the fabricated devices, the GaN layer doping level was 5 × 10^{17}/cm^{-3} and the carrier concentration in ZnO was about 1 × 10^{18}/cm^{-3} based on our previous electrical measurements.[36] Upon applying a DC voltage to metalized arrays of p−n heterojunctions made from ZnO nanowalls on p-GaN, individual heterojunctions in the array independently emit light as can be seen from the electroluminescence (EL) image in Figure 4e. This image was collected from part of a device with a faceted-spiral pattern (inset) containing a millimeter-long ZnO backbone that is under an injection current of ~0.9 mA at +7 V (Supporting Information, Figure S5). Although

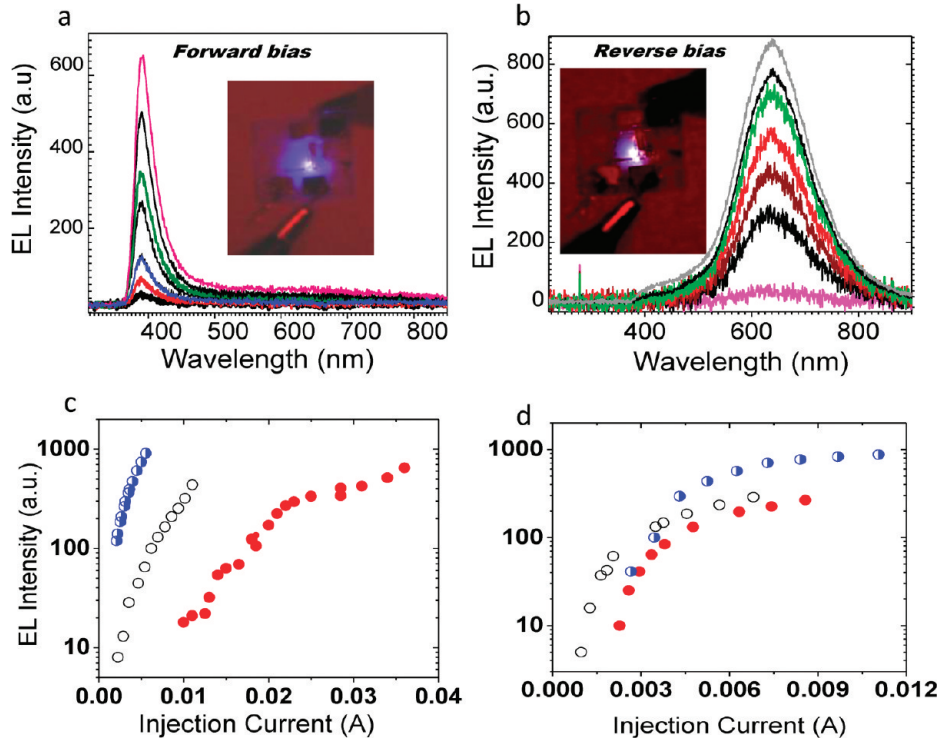

Figure 5. (a) EL spectra of a p−n heterojunction array (similar to the array in Figure 3a) with a lateral dimension of 5 mm under a forward bias of −13 to −25 V (injection current of 0.01−0.036 A). Inset shows the blue emission of the corresponding device at a forward bias of 20 V collected using a digital camera after 30 s of exposure time. (b) EL emission at 640 nm from the same array, but under a reverse bias of +7 to 15 V (0.003−0.011 A injection current). Inset: the orange emission of the same device at a reverse bias of −20 V. (c,d) EL intensity *vs* injected current, respectively, under forward and reverse biases for three different size of nanowall LED arrays (blue circles, 100 μm; white circles, 200 μm; and red circles, 5 mm).

e−h recombination sites are not yet determined along the length of the heterojunctions, our EL results show that both nanowires and nanowalls emit along their entire length in contrast to the mechanically formed p−n junctions where emission originates only from the parts of a nanowire that are in contact with the substrate.[17,18] Another example of a nanowall-based p−n heterojunction array with lateral dimensions of 5 mm × 5 mm and its EL emission is illustrated in Figure 4f. The dark lines in this image are the metal contacts that block some of the emitted light. The strength of this growth technique is in allowing large scale charge injection into planar *nanowire* LEDs with a unique control that is difficult to achieve using other techniques.

To further probe electro-optical characteristics of these heterojunctions, the EL spectra of a number of heterojunction arrays with different shapes and sizes from 100 μm to 5 mm were collected at different voltages from −25 to 27 V using an optical fiber mounted above an active device. Figure 5a illustrates an example in which a series of spectra are collected from a large array of nanowall p−n heterojunctions (EL image shown in Figure 4f) under a forward bias of 9−25 V. The strong excitonic emission of the device at about 390 nm agrees well with the photoluminescence (PL) of ZnO nanowalls at 380 nm (Figure S6) indicating that holes are injected to the n-type ZnO. This is also in agreement with the brightly emitting nanowires in Figure 4e,f showing that the majority of the charge recombination occurs in the ZnO region. The strong emission and the narrow spectral bandwidth (32 nm fwhm) are indicative of a low density of interface states that depress the radiative recombination probability. The inset of Figure 5a shows the blue emission of a 5 mm^2-array of p−n heterojunctions at 20 V with an injection current of 0.017 A. The collective emission of the p−n heterojunctions is intense enough that it can be observed by unaided eye. By moving to reverse bias voltages above 6 V, that is, beyond the break down voltage of the examined devices, we observe a bright orange emission with a wavelength centered at 640 nm (1.95 eV) as shown in the group of spectra in Figure 5b and inset. Although this is still under study, we note that the 640 nm emission intensity decreases as the surface area of the ZnO backbone-GaN decreases. This drop in intensity also coincides with a better rectifying behavior and an increase in the breakdown voltage from 4 V to more than 9 V in smaller size devices (Figure 4c,d). Results suggest that the backbone has a contribution to this emission; nonetheless, we do not observe this emission in the PL of the corresponding devices on GaN. With regard to the electronic states involved in this emission, we tentatively attribute the EL emission under the reverse bias to a transition from an intrinsic shallow state (such as Zn_i) to an intrinsic deep state such as oxygen vacancies.

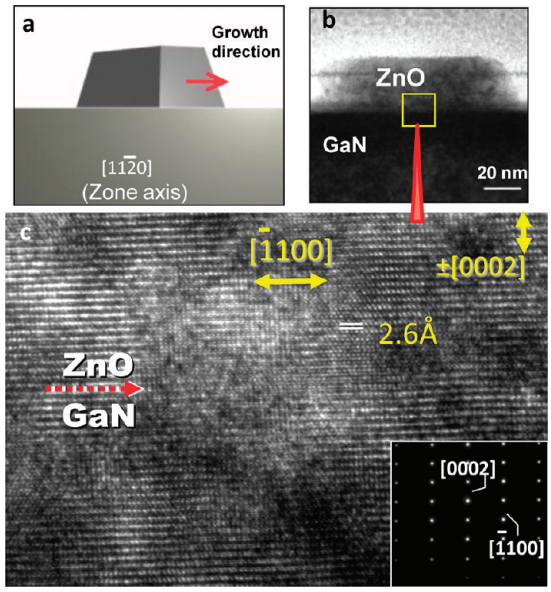

Figure 6. The (a) schematic and (b) TEM image of a ZnO nanowire−GaN interface viewed from [11$\bar{2}$0] zone axis in which the cross-section is 30° tilted relative to the optic axis. (c) HRTEM image of the junction highlighted in panel b and its SAD pattern in the inset. The heterojunction interface is shown with a dashed arrow. The SAD patterns of regions including ZnO, ZnO/GaN interface, and GaN exhibit identical patterns, which highlights the fact that there is an epitaxial relationship between the two crystals with no signs of polycrystalline phases (Supporting Information, Figure S9).

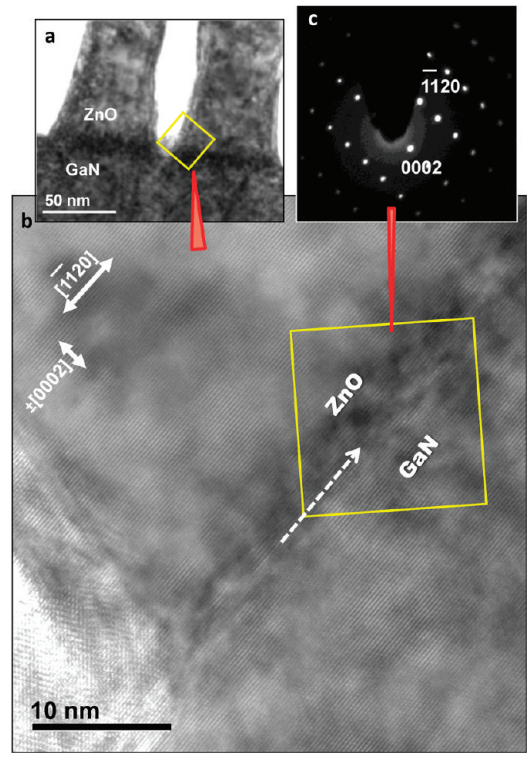

Figure 7. (a) Cross sections of two adjacent ZnO nanowalls grown on GaN; the highlighted area of the interface is further magnified in panel b showing the lattice planes parallel to the interface. (c) The SAD pattern of the marked area of the ZnO−GaN interface demonstrates the directions of *c*- and *a*- planes of ZnO relative to those of GaN.

The shape of the EL emission spectrum does not change by increasing the injection current in both reverse and forward biases. However, as seen in Figure 5c, by increasing the injected current (I) the intensity of the emitted light first grows then reaches a mild saturation at higher voltages. The *ca.* $I-V^2$ relationship obtained under a forward bias (Figure 5c) and start of a diode-saturation at high injection current is observed for three different devices with device sizes of 100 μm, 200 μm, and 5 mm, which could indicate a limited charge carrier concentration at the junction, heating effects, or increase in nonradiative processes. Under a reverse bias condition shown in Figure 5d, a lower current goes through the diodes and EL intensity saturates at much lower currents. Low temperature measurements are underway to better understand the charge recombination mechanisms involved.

The detailed nature of the surface-directed growth of nanowires and resulting heterojunctions was investigated using high resolution transmission electron microscopy (HRTEM) from two different perspectives with zone axes of [**01$\bar{1}$0**] and [**11$\bar{2}$0**]. In the former case, the nanowire cross sections are examined parallel to the growth direction (Supporting Information, Figure S7,S8), while, in the latter, the nanowires are inclined at 30° with respect to the optic axis (Figure 6a), allowing the crystalline structure of the interface along the length of the nanowires to be examined. A representative cross-section of ZnO/GaN nanowire from this perspective is shown in Figure 6b. HRTEM examination of the interface (marked area) and its SAD pattern shown in Figure 6c (and inset) indicate formation of high quality heterojunctions using this growth technique. In the case of ZnO nanowalls, shown in Figure 7a, results show single crystal ZnO grows epitaxially in its ⟨**0001**⟩ axis on c-plane GaN forming vertical ZnO slabs; HRTEM (Figure 7b) reveals nearly coherent and abrupt interfaces without a reaction layer despite the high temperature (900 °C) at which the growth occurs (Supporting Information, Figure S9). In addition, there is no evidence of formation of an amorphous GaO layer at the ZnO−GaN interface, which agrees well with the charge transport measurements. In both nanowires and nanowalls, the orientation relationship of the two crystals relative to each other was determined to be $(0002)_{ZnO}\|(0002)_{GaN}$ and $[\bar{1}100]_{ZnO}\|[\bar{1}100]_{GaN}$ using the electron diffraction data (Figure 7c). Reconstruction of this orientation shows that the lattice commensuration only persists across a few unit cells (Supporting Information, Figure S10); in addition, theory predicts an average distance of 15.8 nm between the misfit dislocations for a fully relaxed ZnO−GaN interface along [**11$\bar{2}$0**] direction.[31] However, in our case, the p−n heterojunctions do not fully exhibit the spacing above and show interfaces with small number of defects such as threading dislocations that are notorious in degrading the device performance of nitride semiconductors.[25] We also observe a detectable amount of strain in the GaN layer under-

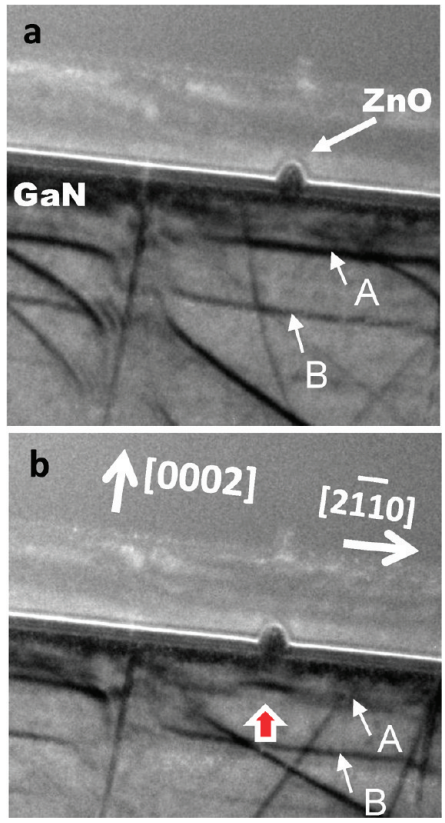

Figure 8. LACBED patterns corresponding to a cross-section of ZnO nanowire−GaN overcoated with a thick layer of amorphous silicon oxide. The pattern contains both local diffraction data and image of the specimen; going from micrograph a to micrograph b upon a slight specimen tilt, the diffraction contours (A and B) shift toward the interface. In graph b, the distorted line (A) reveals the local strain or lattice distortion underneath the nanowire.

neath the ZnO, which is in agreement with the fewer misfit dislocations observed at the interface. The local strain pattern was detected using the large-angle convergent beam electron diffraction (LACBED) technique[37] in which the local diffraction and crystal structural information are overlapped to detect the nanoscale strain (Figure 8). As shown in Figure 8a, when the crystal is oriented such that the diffraction line (A) passes through an area of the GaN that is far from the nanowire interface, the diffraction line remains unperturbed. In contrast, in Figure 8b, when the crystal is tilted slightly so that the contour line (A) now passes through the GaN just beneath the nanowire, it locally becomes distorted (highlighted with the big arrow). The local distortion of the contour is an indication of a localized strain underneath the nanowire.

We explain the lateral growth by viewing the SVLS process as a localized thin film growth process that takes place in a gold nanodroplet with a base area of less than 100 nm^2. Over this small area, the lattice mismatch between the two crystals is minimized by preferential growth in high-symmetry directions, and the stored strain remains below the threshold for the formation of misfit dislocations. As the ZnO nanocrystal is formed, the Au nanodroplet moves forward on GaN and provides more room to the ZnO nanocrystal to elongate. In its further elongation, the ZnO nanocrystal receives its growth program both from the GaN substrate and the ZnO crystal already formed earlier.

In addition to ZnO, we have observed the lateral growth for Ti_2O_3 and GaN on substrates such as Al_2O_3[36] and GaN, which possess hexagonal or trigonal/rhombohedral crystal structures (Supporting Information, Figure S11). We expect to observe the SVLS growth of nanowires using Au for a wide group of materials especially III−V and II−VI semiconductors, since growth of their free-standing forms have already been reported using this process.[24] The present technique maintains the strength of the VLS-based methods in growth of axial and core−shell heterojunctions, while allowing control of their hierarchical assembly. The flexibility in material combination and the ability to grow dense arrays of laterally grown nanowires/nanowalls could lead to the development of novel heterojunctions that are electrically addressable on literally any scale. Because of the unique control over location and orientation of arrays of nanowires afforded by this technique and its compatibility with conventional microfabrication methods, it is expected to impact the field of scalable nanowire-based devices by enabling the realization of numerous structural combinations and device concepts.

METHODS

Growth of Nanowires and Nanowalls. Nanowires are grown by heating a ZnO/graphite mixture (0.15 g, 1:1 mass ratio) loaded on a Si substrate that is positioned at the center of a small quartz tube (13 cm length, 1.9 cm inner diameter). Subsequently, this tube containing an 8 mm^2 gold-patterned GaN substrate is inserted into a tube furnace such that the mixed powder is placed at the center of an outer tube (80 cm length, 4.9 cm inner diameter). The tube furnace temperature is set at 900 °C (with a ramp rate of 110 °C/min) for a variable time of 10−35 min under 0.6 standard liters per minute (SLPM) flow of ultradry N_2 gas (99.99%). c-Plane GaN wafers, 5 μm thick doped with Mg with a concentration of 5×10^{17} cm^{-3}, were purchased from TDI. (Certain commercial equipment, instruments, or materials are identified in this paper to adequately specify the experimental procedure. In no case does such identification imply recommendation or endorsement by the National Institute of Standards and Technology, nor does it imply that the materials or equipment identified are necessarily the best available for the purpose.) Gold patterns were deposited either by dispersing gold nanoparticles 10−40 nm in size or by using a thermal evaporator. The gold film thickness was measured by atomic force microscopy (AFM). Elemental analysis was performed using a Titan 80-300 TEM/STEM (FEI Co.) in parallel (TEM) mode at an accelerating voltage of 300 kV.

Placing Metal Electrodes on Arrays of Nanowires and Nanowalls. GaN substrate is patterned with Au using conventional photolithography, and thus after growth of nanowires their relative coordinates are known. Capitalizing on this advantage, patterns of elec-

trical contacts photolithographically were placed on the ZnO backbones. For metal electrodes connected to the n-type ZnO, Ti (20 nm) and Au (35 nm) and for those on the p-type GaN, Ni (20 nm) and Au (35 nm) were deposited using thermal evaporation.

Electro-optical Measurements. Arrays of p−n heterojunctions of ZnO nanowires or nanowalls on GaN were connected to negative and positive electrodes of a power supply capable of generating voltages up to 70 V. Electroluminescence (EL) of the p−n junctions was collected by placing an optical fiber normal to the device with an optimized working distance, which subsequently guided the emission to a scientific grade CCD for spectral acquisition.

Electrical Measurements. Electrical measurements including two terminal current *vs* source−drain voltage were carried out using (Kiethley 6430) and (Hewlett-Packard 4140B) pico-ammeters and a probe station.

Optical Measurements. For PL measurements, a HeCd laser operating at 325 nm was used to optically excite the ZnO. The laser light was filtered with a Schott Glass UG11 filter to remove unwanted laser emission at 425 nm. Five mW of laser light was focused using a fused silica triplet lens onto an approximately 200 μm diameter spot of the sample at a grazing angle. The ZnO PL was collected through an infinity corrected 40× objective with a numerical aperture of 0.60, which transmits wavelengths above 340 nm. Any residual scattered laser light from the sample was removed using a 325 nm laser blocking filter (optical density = 6). The PL was then focused with a fused silica tube lens onto a charge couple device (CCD) camera used for focusing and imaging the area of interest. Once a suitable region was found, a mirror was placed into the microscope to direct the PL onto the face of a UV-transmitting fused silica fiber. The fiber guided the PL into a spectrometer coupled to a thermoelectrically cooled, scientific grade CCD for spectral acquisition. The PL spectra were collected in the range of 350−900 nm.

FIB Cross-Sectioning. Using a FEI DualBeam instrument, a combination of a focused Ga ion beam and a SEM, electron-transparent cross-sections of horizontally grown nanowires and nanowalls on c-plane gallium nitride were prepared. This technique, which is often called FIB-assisted membrane lift-out, is the best available method in terms of resolution and site specificity for preparing TEM specimens. For this purpose the method described in ref[38] was used.

High Resolution Transmission Electron Microscopy (HRTEM). HRTEM of the nanowire cross-section and nanowall specimens was performed using a Titan 80-300 TEM/STEM (FEI Co.) in parallel (TEM) mode at an accelerating voltage of 300 kV. Zero-loss filtered images were acquired using a Tridiem 865 GIF (Gatan Inc.) with a 10 eV slit. Diffractograms were produced by FFT analysis of the digital images.

Supporting Information Available: Experimental protocols, micrographs of nanowire- and nanowall devices, electrical and optical microscopy characterizations. This material is available free of charge *via* the Internet at http://pubs.acs.org.

REFERENCES AND NOTES

1. Fan, Z.; Ho, J. C.; Jacobson, Z. A.; Razavi, H.; Javey, A. Large-Scale, Heterogeneous Integration of Nanowire Arrays for Image Sensor Circuitry. *Proc. Natl. Acad. Sci. U.S.A.* **2008**, *105*, 11066.
2. Duan, X.; Niu, C.; Sahi, V.; Chen, J.; Parce, J. W.; Empedocles, S.; Goldman, J. L. High-Performance Thin-Film Transistors Using Semiconductor Nanowires and Nanoribbons. *Nature* **2003**, *425*, 274–278.
3. Goldhaber-Gordon, D.; Montemerlo, M. S.; Love, J. C.; Opiteck, G. J.; Ellenbogen, J. C. Overview of Nanoelectronic Devices. *Proc. IEEE* **1997**, *85*, 521–540.
4. Bjork, M. T.; Ohlsson, B. J.; Sass, T.; Persson, A. I.; Thelander, C.; Magnusson, M. H.; Deppert, K.; Wallenberg, L. R.; Samuelson, L. One-Dimensional Steeplechase for Electrons Realized. *Nano Lett.* **2002**, *2*, 87–89.
5. Qian, F.; Li, Y.; Gradecak, S.; Park, H.-G.; Dong, Y.; Ding, Y.; Wang, Z. L.; Lieber, C. M. Multi-quantum-Well Nanowire Heterostructures for Wavelength-Controlled Lasers. *Nat. Mater.* **2008**, *7*, 701–706.
6. Lauhon, L. J.; Gudiksen, M. S.; Wang, D.; Lieber, C. M. Epitaxial Core-Shell and Core-Multishell Nanowire Heterostructures. *Nature* **2002**, *420*, 57–61.
7. Yang, C.; Zhong, Z.; Lieber, C. M. Encoding Electronic Properties by Synthesis of Axial Modulation-Doped Silicon Nanowires. *Science* **2005**, *310*, 1304–1307.
8. Gudiksen, M. S.; Lauhon, L. J.; Wang, J.; Smith, D. C.; Lieber, C. M. Growth of Nanowire Superlattice Structures for Nanoscale Photonics and Electronics. *Nature* **2002**, *415*, 617–620.
9. Morales, A. M.; Lieber, C. M. A Laser Ablation Method for the Synthesis of Crystalline Semiconductor Nanowires. *Science* **1998**, *279*, 208–211.
10. Wang, X.; Song, J.; Li, P.; Ryou, J. H.; Dupuis, R. D.; Summers, C. J.; Wang, Z. L. Growth of Uniformly Aligned ZnO Nanowire Heterojunction Arrays on GaN, AlN, and $Al_{0.5}Ga_{0.5}N$ Substrates. *J. Am. Chem. Soc.* **2005**, *127*, 7920–7923.
11. Tian, B.; Xie, P.; Kempa, T. J.; Bell, D. C.; Lieber, C. M. Single-Crystalline Kinked Semiconductor Nanowire Superstructures. *Nat. Nano* **2009**, *4*, 824–829.
12. Xiang, B.; Wang, P.; Zhang, X.; Dayeh, S. A.; Aplin, D. P. R.; Soci, C.; Yu, D.; Wang, D. Rational Synthesis of p-Type Zinc Oxide Nanowire Arrays Using Simple Chemical Vapor Deposition. *Nano Lett.* **2006**, *7*, 323–328.
13. Sun, X. W.; Huang, J. Z.; Wang, J. X.; Xu, Z. A ZnO Nanorod Inorganic/Organic Heterostructure Light-Emitting Diode Emitting at 342 nm. *Nano Lett.* **2008**, *8*, 1219–1223.
14. Zhang, X.-M.; Lu, M.-Y.; Zhang, Y.; Chen, L. J.; Wang, Z. L. Fabrication of a High-Brightness Blue-Light-Emitting Diode Using a ZnO-Nanowire Array Grown on p-GaN Thin Film. *Adv. Mater.* **2009**, *21*, 2767–2770.
15. Kim, H.-M.; Cho, Y.-H.; Lee, H.; Kim, S. I.; Ryu, S. R.; Kim, D. Y.; Kang, T. W.; Chung, K. S. High-Brightness Light Emitting Diodes Using Dislocation-Free Indium Gallium Nitride/Gallium Nitride Multiquantum-Well Nanorod Arrays. *Nano Lett.* **2004**, *4*, 1059–1062.
16. Tian, B.; Zheng, X.; Kempa, T. J.; Fang, Y.; Yu, N.; Yu, G.; Huang, J.; Lieber, C. M. Coaxial Silicon Nanowires as Solar Cells and Nanoelectronic Power Sources. *Nature* **2007**, *449*, 885–889.
17. Zimmler, M. A.; Stichtenoth, D.; Ronning, C.; Yi, W.; Narayanamurti, V.; Voss, T.; Capasso, F. Scalable Fabrication of Nanowire Photonic and Electronic Circuits Using Spin-on Glass. *Nano Lett.* **2008**, *8*, 1695–1699.
18. Lee, S. K.; Kim, T. H.; Lee, S. Y.; Choi, K. C.; Yang, P. High-Brightness Gallium Nitride Nanowire UV and Blue Light Emitting Diodes. *Philos. Mag.* **2007**, *87*, 2105–2115.
19. Kim, F.; Kwan, S.; Akana, J.; Yang, P. Langmuir−Blodgett Nanorod Assembly. *J. Am. Chem. Soc.* **2001**, *123*, 4360–4361.
20. Yu, G.; Cao, A.; Lieber, C. M. Large-Area Blown Bubble Films of Aligned Nanowires and Carbon Nanotubes. *Nat. Nano* **2007**, *2*, 372–377.
21. Melosh, N. A.; Boukai, A.; Diana, F.; Gerardot, B.; Badolato, A.; Petroff, P. M.; Heath, J. R. Ultrahigh-Density Nanowire Lattices and Circuits. *Science* **2003**, *300*, 112–115.
22. Javey, A.; Nam; Friedman, R. S.; Yan, H.; Lieber, C. M. Layer-by-Layer Assembly of Nanowires for Three-Dimensional, Multifunctional Electronics. *Nano Lett.* **2007**, *7*, 773–777.
23. Nikoobakht, B.; Michaels, C. A.; Stranick, S. J.; Vaudin, M. D. Horizontal Growth and "*in Situ*" Assembly of Oriented Zinc Oxide Nanowires. *Appl. Phys. Lett.* **2004**, *85*, 3244–3246.
24. Fortuna, S. A.; Wen, J.; Chun, I. S.; Li, X. Planar GaAs Nanowires on GaAs (100) Substrates: Self-Aligned, Nearly Twin-Defect Free, and Transfer-Printable. *Nano Lett.* **2008**, *8*, 4421–4427.
25. Kozodoy, P.; Ibbetson, J. P.; Marchand, H.; Fini, P. T.; Keller, S.; Speck, J. S.; DenBaars, S. P.; Mishra, U. K. Electrical Characterization of GaN p−n Junctions with and without Threading Dislocations. *Appl. Phys. Lett.* **1998**, *73*, 975–977.

26. Vispute, R. D.; Talyansky, V.; Choopun, S.; Sharma, R. P.; Venkatesan, T.; He, M.; Tang, X.; Halpern, J. B.; Spencer, M. G.; Li, Y. X.; *et al*. Heteroepitaxy of ZnO on GaN and Its Implications for Fabrication of Hybrid Optoelectronic Devices. *Appl. Phys. Lett.* **1998**, *73*, 348–350.
27. Wang, Z. L.; Song, J. Piezoelectric Nanogenerators Based on Zinc Oxide Nanowire Arrays. *Science* **2006**, *312*, 242–246.
28. Nomura, K.; Ohta, H.; Ueda, K.; Kamiya, T.; Hirano, M.; Hosono, H. Thin-Film Transistor Fabricated in Single-Crystalline Transparent Oxide Semiconductor. *Science* **2003**, *300*, 1269–1272.
29. Law, M.; Greene, L. E.; Johnson, J. C.; Saykally, R.; Yang, P. Nanowire Dye-Sensitized Solar Cells. *Nat. Mater.* **2005**, *4*, 455–459.
30. Pearton, S. J.; Lim, W. T.; Wright, J. S.; Tien, L. C.; Kim, H. S.; Norton, D. P.; Wang, H. T.; Kang, B. S.; Ren, F.; Jun, J.; *et al*. ZnO and Related Materials for Sensors and Light-Emitting Diodes. *J. Electron. Mater.* **2008**, *37*, 1426–1432.
31. Levin, I.; Davydov, A.; Nikoobakht, B.; Sanford, N.; Mogilevsky, P. Growth Habits and Defects in ZnO Nanowires Grown on GaN/Sapphire Substrates. *Appl. Phys. Lett.* **2005**, *87*, 103110103110−3.
32. Haraguchi, K.; Katsuyama, T.; Hiruma, K.; Ogawa, K. GaAs p−n Junction Formed in Quantum Wire Crystals. *Appl. Phys. Lett.* **1991**, *60*, 745–747.
33. Wagner, R. S.; Ellis, W. C. Vapor−Liquid−Solid Mechanism of Single Crystal Growth. *Appl. Phys. Lett.* **1964**, *4*, 89–90.
34. Hannon, J. B.; Kodambaka, S.; Ross, F. M.; Tromp, R. M. The Influence of the Surface Migration of Gold on the Growth of Silicon Nanowires. *Nature* **2006**, *440*, 69–71.
35. Wang, Z. L.; Kong, X. Y.; Zuo, J. M. Induced Growth of Asymmetric Nanocantilever Arrays on Polar Surfaces. *Phys. Rev. Lett.* **2003**, *91*, 185502.
36. Nikoobakht, B. Toward Industrial-Scale Fabrication of Nanowire-Based Devices. *Chem. Mater.* **2007**, *19*, 5279–5284.
37. Tanaka, M.; Saito, R.; Ueno, K.; Harada, Y. Large-Angle Convergent-Beam Electron-Diffraction. *J. Electron Microsc.* **1980**, *29*, 408–412.
38. Nikoobakht, B.; Eustis, S.; Herzing, A. Strain-Driven Growth of Zinc Oxide Nanowires on Sapphire: Transition from Horizontal to Standing Growth. *J. Phys. Chem. C* **2009**, *113*, 7031–7037.